NANO LETTERS

LETTER

pubs.acs.org/NanoLett

Strain Patterning and Direct Measurement of Poisson's Ratio in Nanoparticle Monolayer Sheets

Pongsakorn Kanjanaboos,[†] Alexandra Joshi-Imre,[‡] Xiao-Min Lin,[‡] and Heinrich M. Jaeger*[,†]

[†]James Franck Institute and Department of Physics, The University of Chicago, Chicago, Illinois 60637, United States

[‡]Center for Nanoscale Materials, Argonne National Laboratory, Argonne, Illinois 60439, United States

Supporting Information

ABSTRACT: Close-packed monolayers self-assembled from ligated nanoparticles can form 10 nm thin sheets that stretch over micrometer-wide holes. Employing electron and focused ion beams, we show that one can locally tailor the strain in such sheets while they remain clamped around their perimeter, making it possible to imprint strain fields by design. Furthermore, using the nanoparticles themselves to track imposed strain gradients allows for the first direct measurement of Poisson's ratio in these two-dimensional materials.

KEYWORDS: Gold nanoparticles, freestanding membrane, electron beam irradiation, focused ion beam, mechanical properties, strain, self-assembly

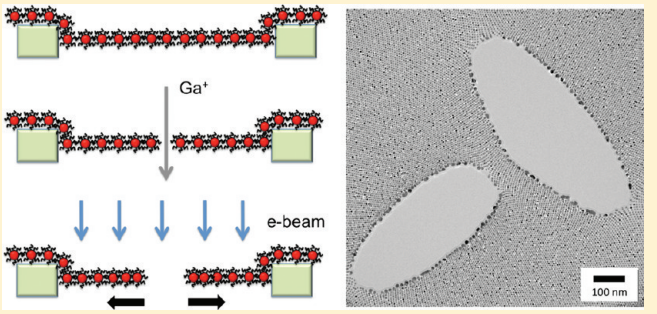

Recent experimental advances have made it possible to self-assemble nanoparticles into freestanding ultrathin sheets.[1−11] With ligated nanoparticles as building blocks, the choice of material and size for particle cores as well as ligands provides a means to tailor the sheets' structural properties, including the option of binary superlattices,[8] independently from their electronic,[11] magnetic,[8] or mechanical[2,7,9] functionality. Despite the short length of typical ligands, close-packed monolayer sheets exhibit surprisingly large Young's moduli of several GPa,[2,7,9] values that can be attributed to ligand interdigitation and strong confinement in the interstices between particles.[9,12,13] This combination of versatility and robustness makes such sheets promising candidates for the investigation of substrate-free transport phenomena and for sensing applications.[7,11]

A freestanding, close-packed monolayer represents the ultimate two-dimensional limit of a nanoparticle-based solid. Mechanically, the layer resembles a lattice of springs, with effectively rigid, inorganic particle cores connected to their six nearest neighbors via short "springs" formed by ligands that bind together due to van der Waals forces.[13] When such layer is stretched isotropically and then clamped down around its edges like a drumhead, a state of uniform initial strain is generated. Prior work established several self-assembly techniques that either organize nanoparticles into a sheet at a liquid−air interface and then dry or transfer the sheet onto a substrate with a prefabricated hole,[2,8,9] or directly form the sheet inside the hole.[6,7] Where the sheet sticks to the substrate it becomes immobilized, while the freestanding portion extending across the hole shrinks slightly as any remaining solvent evaporates. This leads to taut monolayer sheets that can extend across holes many micrometers in diameter and exhibit tensile prestrains of a few tenths of a percent.[2,9] Luo and co-workers observed that when such monolayer sheets rip (typically around the edges of the hole), some of the prestrain is relaxed and the interparticle spacing decreases along directions of reduced tension.[6] This suggests that freestanding nanoparticle layers should respond to changes in the boundary conditions similar to thin elastic sheets.

Here we exploit this behavior to show that the ligand-mediated coupling between nanoparticles provides unique opportunities to manipulate monolayer sheets deliberately and in a controlled way. We demonstrate how the combined action of locally removing some and globally tensioning the remaining "springs" can be used to engineer anisotropic strain patterns that change the interparticle spacing with precision, while keeping the overall sheet taut and firmly clamped around its perimeter. Furthermore, tracking the local displacement of individual nanoparticles in situ as the sheet adjusts to changes in the boundary conditions, we extract Poisson's ratio directly. By contrast, all previous work focusing on mechanical properties such as the Young's modulus measured the response to applied stresses and therefore had to assume Poisson's ratio.[2,6,7,9,10]

The main idea behind our approach is the use of a focused ion beam to surgically cut slits into the clamped sheet (or remove portions of the sheet), thereby relaxing some of the initial prestrain in the vicinity of the cut. In a second step, we expose the sheet to an electron beam, which does not change the local topology but is found to have an effect similar to further tensioning the whole sheet around its outer, clamped rim.

Received: May 4, 2011
Published: May 20, 2011

dx.doi.org/10.1021/nl2014873 | *Nano Lett.* 2011, 11, 2567–2571

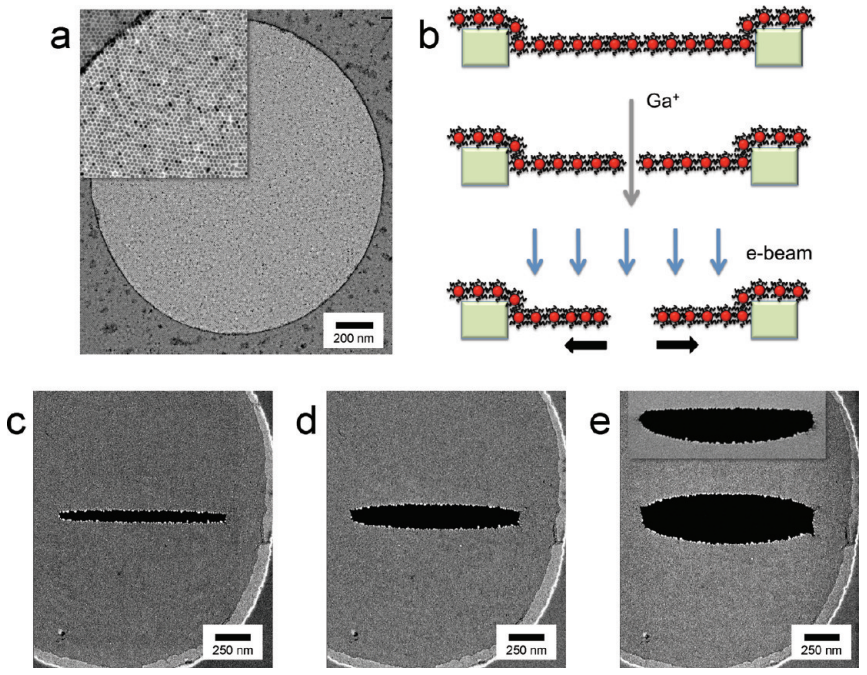

Figure 1. Manipulation of freestanding, monolayer nanoparticle sheets by ion and electron beams. (a) TEM image of monolayer stretched across 1.6 μm diameter hole prefabricated in 100 nm thick silicon nitride. Inset: Zoomed-in view showing individual nanoparticles. (b) Schematic cross sections showing the uncut sheet (top), a slit cut by the focused ion beam (middle), and the subsequent widening of the slit induced by exposure of the sheet to electrons during SEM imaging (bottom). (c−e) The slit after the 2nd (c), 7th (d), and 39th (e) SEM scan, applying a uniform dose of 4 mC/cm^2 per scan. The inset in (e) shows the asymmetric widening if only the lower portion of the slit is exposed to the electon beam.

Figure 1 shows the key steps involved in our experiments. We start with a highly ordered nanoparticle monolayer sheet that was self-assembled from solution and draped over a hole (~2 μm diameter) prefabricated by reactive ion etching into a 100 nm thick SiN membrane. For the results described here, we used 5.5 nm diameter gold nanocrystals ligated with dodecanethiol, but freestanding layers can also be formed with other core/ligand combinations.[6,8,9] Details of the preparation process have been described elsewhere.[2,9] Briefly, we deposit a water droplet over a substrate with one or more holes, and add a droplet of toluene solution containing the gold nanoparticles. A compact monolayer quickly forms at the water−toluene interface as the toluene evaporates. Since the water diffuses much more slowly through the monolayer, the layer gently drapes itself across the holes, creating freestanding sheets that are clamped to the substrate around their perimeter by van der Waals forces (Figure 1a). As confirmed in earlier work[2,9] by atomic force microscopy and indicated in Figure 1b, the sheets recede into the holes.

Next a Ga^+ ion beam, focused down to a few interparticle spacings, is used to cut through the sheet. Figure 1c shows the slit resulting from a ~50 nm-wide line cut, imaged in situ by the scanning electron microscope (SEM) attached to our focused ion beam (FIB) system (FEI Nova NanoLab). This cut removed 7−8 rows of particles. Melting and coalescence of nanoparticles due to the ion beam is seen to be confined to particles along the perimeter of the cut and does not extend more than ~10 nm into the sheet. In the following, we limit our discussion to results obtained with narrow slits, but other shapes or more complex cutouts are of course possible.

An initially surprising finding was that imaging with the SEM introduces additional tension into the sample, equivalent to increasing the global prestrain of the sheet beyond its drying-induced value. This is shown by Figure 1c−e, which demonstrates the gradual expansion of the size of the gap produced by the slit as the overall deposited e-beam dose increases (see Supporting Information for a movie compiled from 45 successive exposures). Note that perpendicular to the slit the gap widens significantly while it changes much less along the slit where the stress concentration is high, as expected from an elastic membrane that is radially tensioned. That this tensioning is directly due to the dosing of the sheet with electrons is confirmed by performing the SEM scanning over only half the slit for some time and then zooming out to find that the side of the slit that received the higher dose expanded more (Figure 1e, inset).

We track the amount of strain introduced by the e-beam in two ways (Figure 2). First, we can simply measure changes in the macroscopic features of the evolving slit shape. In particular, the maximum gap size of a long slit directly indicates the amount of strain in the sheet. The data from two samples in Figure 2a demonstrate the repeatability of the exposure process, and the curvature makes clear that the effect becomes weaker at higher net dose, eventually saturating. Second, from the diffraction pattern computed by 2D fast Fourier transformation (FFT) of a small patch of the sample we can observe the evolution of the local strain field (Figure 2b,c). Since close-packed nanoparticles form a triangular lattice, this method can follow the three independent lattice directions found in a particular patch of the sample; data for other angles are obtained by selecting patches with different local lattice orientations (e.g., on different samples or different portions of the same sample).

Just above the center of a long slit (see box in Figure 2b), the sheet will experience essentially uniaxial compression perpendicular

dx.doi.org/10.1021/nl2014873 |*Nano Lett.* 2011, 11, 2567–2571

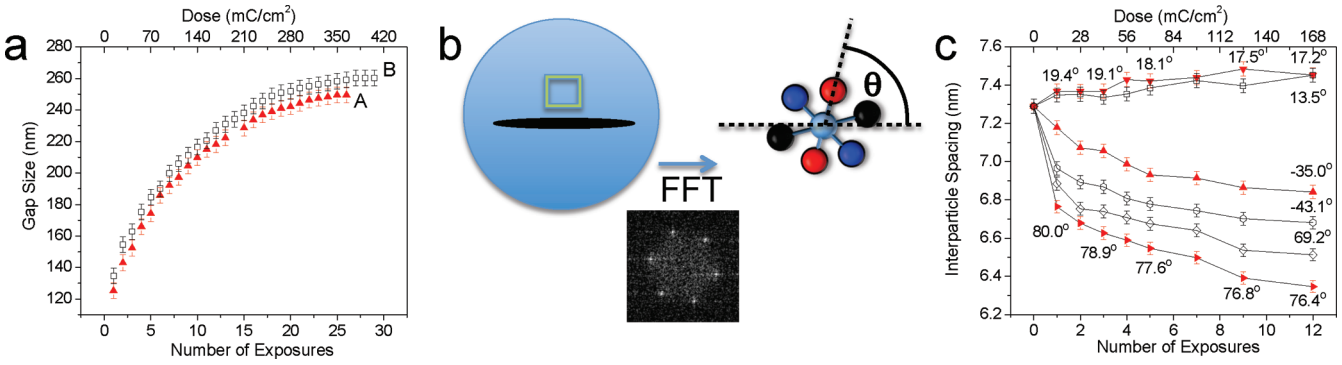

Figure 2. Strain tracking as a function of applied electron-beam dose. Each SEM scan corresponds to a uniform dose of 14mC/cm^2, applied at 5 keV. (a) Evolution of the gap size, defined as the vertical length of the opening at the center of the slit in Figure 1c−e. (b) Procedure used to track the lattice deformation by monitoring changes in the positions and angles of the peaks in 2D FFT patterns of a local patch of the SEM image, indicated by the box. The sketch of the real space particle lattice on the right defines the angle θ with respect to the long slit axis. (c) Interparticle spacing as a function of e-beam dose at several angles θ, obtained from a 20 × 20 particle patch above the middle of the slit. As the particle lattice deforms due to the applied strain, the angles between between nearest neighbors also change. For two traces, this is indicated at every other data point; the θ values listed for the other traces correspond to the angle after 12 exposures. The labels A and B denote the same samples in Figure 2a,c and Figure 3.

to the cut. The data in Figure 2c, obtained from an area containing roughly 20 × 20 particles, show the resulting shrinking of the interparticle spacing along the direction of compression as well as the concomitant expansion parallel to the slit. The initial change in the spacing is due to both the relaxation of the drying-induced prestrain by the FIB cut and the subsequent e-beam dose applied during the first SEM scan. With further exposure, the local particle lattice is seen to continue to deform, but the amount of change tapers off as already observed in Figure 2a for the maximum gap size of the slit as a whole.

As a number of studies of self-assembled alkanethiol films on gold surfaces have shown,[14−16] e-beam exposure affects the molecules both by damage and structural changes to their backbone, including fragmentation and cross-linking, and by severing the sulfur bond with the gold core. Zharnikov and Grunze point out[14] that this leads to two opposing effects: on the one hand a thinning-out coupled with increased reactivity, and on the other hand the emergence of a tough, glassy structure due to cross-linking. A likely scenario for the strain-inducing behavior we find therefore proceeds as follows. In close-packed arrays of Au nanoparticles with highly interdigitated ligands, since interparticle gap distances barely exceed the length of alkanethiol chains, the e-beam initially thins out the ligands, allowing them to contract; however, increased cross linking eventually counteracts further contraction, thereby leading to the saturation seen in Figure 2a and c.

This scenario predicts that inverting the procedure, that is, first exposing the sheet to the e-beam and then performing the cut, should lead to significantly smaller opening of the slit, which is indeed what we observe (see Supporting Information, Figure S3). It is also in line with prior findings[4,17−19] that sufficiently large e-beam doses, around 10 mC/cm^2 at 10−30 keV, turn dodecanethiol-ligated Au nanoparticle layers into negative resists. Moreover, even at the very large doses shown in Figure 2a, we did not observe significant particle coalescence (see also below), which implies that desorption of ligand fragments becomes less likely and formation of tough cross-linked bundles more likely with prolonged exposure.

The data in Figure 2c provide direct access to Poisson's ratio, $\nu = -d\varepsilon_{trans}/d\varepsilon_{axial}$, where the infinitesimal strain $d\varepsilon = dL/L$ is

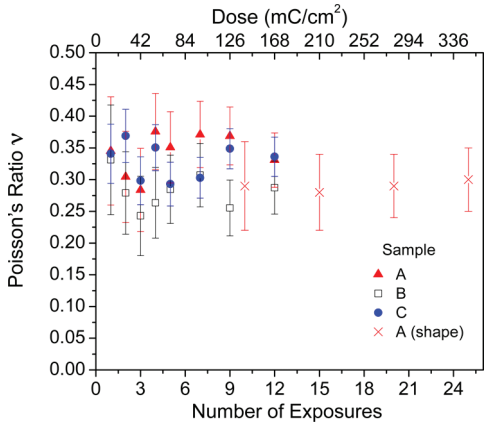

Figure 3. Poisson's ratio ν as a function of applied electron-beam dose. Values for ν for three samples were calculated from data as in Figure 2c together with the corresponding angles at each dose value. Additional data (crosses) out to higher doses were obtained for one of the samples by matching simulations to the shape of the gap (see text and Supporting Information for details).

the relative change in particle center-to-center spacing L along the direction of axial compression (θ = 90° in Figure 2b) or transverse expansion (θ = 0). Integrating the infinitesimal strain up to the net value $\Delta L/L_0$ associated with a paricular dose, we have $\nu = -\log(1 + \Delta L_{trans}/L_{0,trans})/\log(1 + \Delta L_{axial}/L_{0,axial})$. Here $\Delta L_{trans} > 0$ and $\Delta L_{axial} < 0$ are the measured changes in particle spacing projected onto the θ = 0 and 90° directions, and $L_{0,trans}$ and $L_{0,axial}$ similarly are the projections of the spacing, L_0 = 7.3 nm, in the unperturbed sheet (measured away from the cut, near the clamped rim).

The resulting values for Poisson's ratio as a function of dose are shown in Figure 3 for three samples (see Supporting Information for details on the calculation). There are some variations among individual samples, but within the experimental error of ±15% the data appear independent of dose up to a dozen SEM exposures and cluster around an average value ν = 0.32 ± 0.02.

For larger doses sample charging starts to compromise the quality of the SEM images and we lose the ability to follow local

dx.doi.org/10.1021/nl2014873 |Nano Lett. 2011, 11, 2567–2571

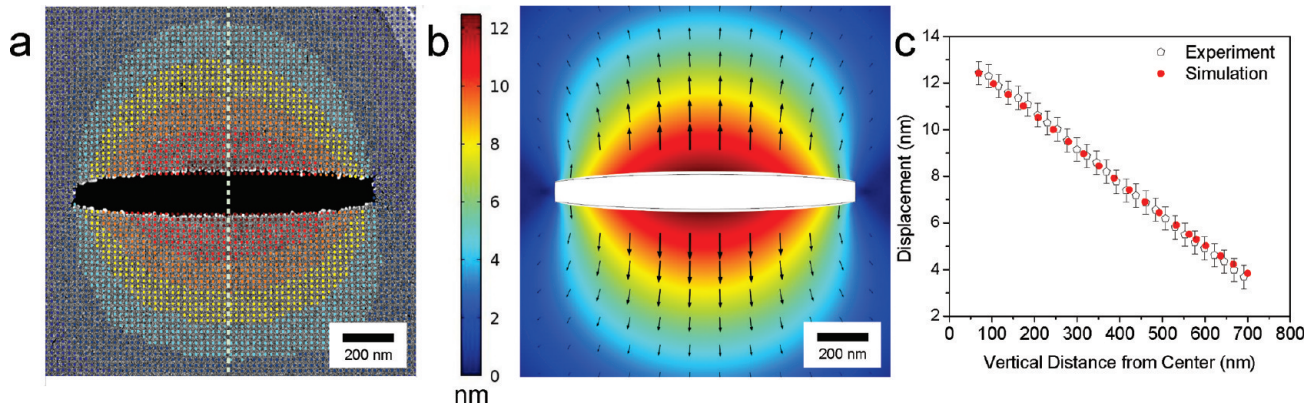

Figure 4. Modeling nanoparticle monolayers as uniformly tensioned, two-dimensional linear elastic sheets. (a) Displacement field calculated by correlating images of the 4th and 7th SEM exposure. Color indicates the displacement magnitude (2 nm bins). The background image shows the 7th exposure. (b) Simulated displacement field after the 7th exposure for a 2D elastic sheet with the same slit geometry, hole shape, and clamped boundary conditions as the experiment in (a), using $\nu = 0.32$. The outline of the slit after the 4th exposure is shown as a thin black line. The color scale is the same for (a) and (b). (c) Comparison of measured and simulated displacements ΔL between 7th and 4th exposure, taken along the dotted vertical line through the center of the slit in (a).

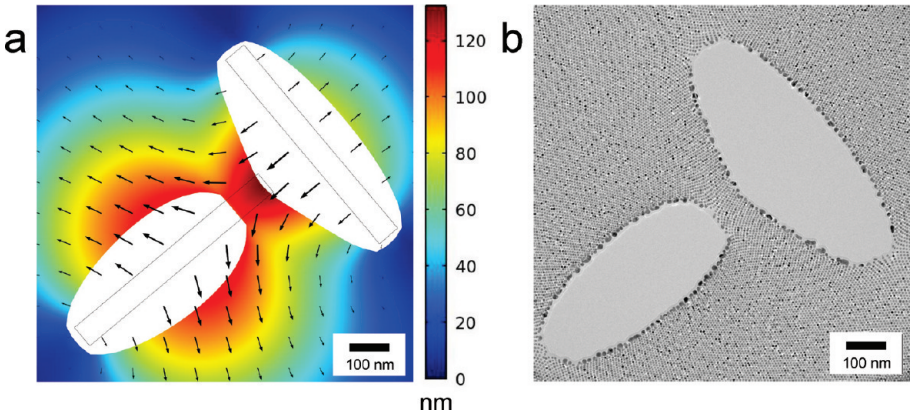

Figure 5. Strain patterns by design. As an example, a pattern produced by two perpendicular slits, each 600 nm long and 60 nm wide, is shown. (a) Simulated displacement field for 12% uniform, radial prestrain. (b) TEM image of nanoparticle sheet after >50 SEM scans at 4 mC/cm^2 per scan. Note the direct correspondence between gradients in the computed displacement field and the gradients observed in the interparticle spacing.

changes in particle spacing with precision. However, we can also track the shape of the gap as a whole which, assuming a 2D elastic sheet, for a given cut geometry and strain along the hole perimeter is uniquely determined by Poisson's ratio. While not as accurate as the local method, this allows us to obtain estimates for ν up to doses of ~350 mC/cm^2 by performing simulations (COMSOL Multiphysics) and adjusting ν and the strain to give the best match of the gap size and shape to the experiments. These data, shown as crosses in Figure 3, while slightly lower than the ones obtained from the computed local diffraction patterns for the same sample, further support the notion that ν is not affected by e-beam exposure.

This dose independence of the Poisson ratio can be traced to the underlying lattice structure of the nanoparticle sheet. In a simple triangular lattice, where each node is connected to its nearest neighbors by six radial springs of stiffness α, the Poisson ratio is a property of the local network topology only and has a value of one-third, independent of α.[20,21] When additional angular springs are included between the radial ones, Wang and co-workers showed[21] that the Poisson ratio becomes $\nu = (1 - 3(\beta/L_0^2)/\alpha)/(3 + 3(\beta/L_0^2)/\alpha)$, where β/L_0^2 is the effective angular spring stiffness in response to torque applied at L_0, the nearest neighbor distance. Within this picture, the average value $\nu \approx 0.32$ implies $(\beta/L_0^2)/\alpha \approx 0.01$. In either case, as long as the e-beam changes the interstitial material uniformly across the exposed area, we can expect ν to remain constant. The role of the underlying network comes into focus when comparing the triangular to a honeycomb lattice such as single layer graphene, where simulations predict Poisson ratios ~0.6 (although there is considerable variation among literature values depending on assumptions about the stiffness of the C−C bonds and direct measurements exist only for bulk samples or flakes).[22]

Knowing the Poisson ratio, we next test whether the whole nanoparticle monolayer can indeed be treated as a uniformly tensioned elastic sheet. To this end, we obtain the full 2D displacement field by locally correlating SEM images from successive exposures and compare it to simulations of an isotropic 2D elastic membrane with $\nu = 0.32$. As Figure 4 shows, the experimental data and simulations match remarkably well. As an example of the quantitative agreement, in Figure 4c we directly compare the measured and computed relative displacements along a vertical line scan through the center of the slit. From these data, the additional strain induced by the e-beam between

dx.doi.org/10.1021/nl2014873 |*Nano Lett.* 2011, 11, 2567–2571

the fourth and seventh exposures was 1.3% in the central region just above the slit (0.9% global strain).

In a slit, stresses are concentrated near regions of high curvature. As the global tension is increased by the e-beam exposure, small fractures are seen to emerge at the corners of the FIB cut (Figure 1c−e). However, these fractures do not propagate far and the sheet does not tear apart. Correlating simulations as in Figure 4 with SEM images just before the apperance of a fracture, and using previously published[9] values for the mean Young's modulus, $E \approx 4$ GPa, in nonirradiated monolayer sheets, we estimate 100 MPa as a lower bound for the local fracture stress. This value compares favorably with tensile yield stresses in polymer-based nanomembranes.[10,23]

These results suggest a path toward implementing a wide variety of complex, anisotropic strain patterns using only two ingredients: judiciously placed cuts (via the FIB) followed by a predetermined amount of tensioning (via the SEM). In practical applications, this is further simplified by two unique features of close-packed nanoparticle sheets; since the e-beam-induced tensioning saturates at large doses (Figure 2a) and the Poisson ratio remains constant (Figure 3), the large-dose limit always produces a well-defined asymptotic pattern. Figure 5 exemplifies this for a strain field designed by placing two cuts at right angles to each other. In this case, the only input into the simulation (Figure 5a) besides the cut geometry was $\nu = 0.32$ and the total amount of equivalent prestrain provided by the e-beam exposure. The sample in this case was exposed to >50 SEM imaging cycles, that is, it reached the saturation limit (Figure 2a). Note that subsequent imaging by transmission electron microscopy (TEM) did not induce further changes in particle spacing nor lead to particle coalescence, confirming the notion that extensive cross-linking had already turned the interstitial material glassy. Comparing the simulation with the TEM image of the sample (Figure 5b) demonstrates how well the local strain gradients, made visible by the distortions of the close-packed lattice of particles, follow the prediction from 2D linear elastic theory.

In summary, we have shown the strain field can be manipulated in a self-assembled freestanding nanoparticle membrane using focused ion beams and scanning electron microscopy. The ability to control local variations in interparticle spacing opens up new possibilities to tune the interparticle coupling for magnetic, electronic, and photonic applications. In the examples discussed (except Figure 1e, inset), the radiation was applied uniformly. Extensions to nonuniform, local exposure or dose gradients are easily possible and could be used to further enhance the range of imprintable strain patterns.

■ ASSOCIATED CONTENT

Ⓢ Supporting Information. Detailed information on the techniques used as well as a movie compiled from a sequence of SEM images as in Figures 1c−e, showing the evolution of the slit shape as it is opening up under e-beam exposure. This material is available free of charge via the Internet at http://pubs.acs.org.

■ AUTHOR INFORMATION

Corresponding Author

*Ph: 773 702-6074. E-mail: h-jaeger@uchicago.edu.

■ ACKNOWLEDGMENT

We thank E. Brown, E. Efrati, J. Freed-Brown, J. He, M. Miskin, and W. Zhang for helpful discussions, A. Athanassiadis for assistance with the simulations, and R. Divan, Y. Chen, and Q. Guo for technical assistance. This work was supported by the NSF through DMR-0907075. The Chicago MRSEC, supported by NSF under DMR-0820054, is gratefully acknowledged for access to its shared experimental facilities. The work at Argonne was supported by the U.S. Department of Energy (DOE), BES-Materials Sciences, under Contract No. DE-AC02-06CH11357, and by the DOE Center for Nanoscale Materials.

■ REFERENCES

(1) Lin, Y.; Skaff, H.; Boker, A.; Dinsmore, A. D.; Emrick, T.; Russell, T. P. *J. Am. Chem. Soc.* **2003**, *125*, 12690.
(2) Mueggenburg, K. E.; Lin, X. M.; Goldsmith, R. H.; Jaeger, H. M. *Nat. Mater.* **2007**, *6*, 656.
(3) Okamura, Y.; Utsunomiya, S.; Suzuki, H.; Niwa, D.; Osaka, T.; Takeoka, S. *Colloids Surf., A* **2008**, *318*, 184.
(4) Pang, J. B.; Xiong, S. S.; Jaeckel, F.; Sun, Z. C.; Dunphy, D.; Brinker, C. J. *J. Am. Chem. Soc.* **2008**, *130*, 3284.
(5) Xia, H.; Wang, D. *Adv. Mater.* **2008**, *20*, 4253.
(6) Cheng, W. L.; Campolongo, M. J.; Cha, J. J.; Tan, S. J.; Umbach, C. C.; Muller, D. A.; Luo, D. *Nat. Mater.* **2009**, *8*, 519.
(7) Cheng, W. L.; Campolongo, M. J.; Cha, J. J.; Tan, S. J.; Umbach, C. C.; Muller, D. A.; Luo, D. *Nano Today* **2009**, 482.
(8) Dong, A.; Chen, J.; Vora, P. M.; Kikkawa, J. M.; Murray, C. B. *Nature* **2010**, *466*, 474.
(9) He, J.; Kanjanaboos, P.; Frazer, N. L.; Weis, A.; Lin, X. M.; Jaeger, H. M. *Small* **2010**, *6*, 1449.
(10) Long, R.; Hui, C.-Y.; Cheng, W.; Campolongo, M.; Luo, D. *Nanoscale Res. Lett.* **2010**, *5*, 1236.
(11) Liao, J.; Zhou, Y.; Huang, C.; Wang, Y.; Peng, L. *Small* **2011**, *7*, 583.
(12) Landman, U.; Luedtke, W. D. *Faraday Discuss.* **2004**, *125*, 1.
(13) Schapotschnikow, P.; Pool, R.; Vlugt, T. J. H. *Nano Lett.* **2008**, *8*, 2930.
(14) Zharnikov, M.; Grunze, M. *J. Vac. Sci.Technol., B* **2002**, *20*, 1793.
(15) Duwez, A. S. *J. Electron Spectrosc. Relat. Phenom.* **2004**, *134*, 97.
(16) Zhou, C.; Trionfi, A.; Hsu, J. W. P.; Walker, A. V. *J. Phys. Chem. C* **2010**, *114*, 9362.
(17) Lin, X. M.; Parthasarathy, R.; Jaeger, H. M. *Appl. Phys. Lett.* **2001**, *78*, 1915.
(18) Werts, M. H. V.; Lambert, M.; Bourgoin, J. P.; Brust, M. *Nano Lett.* **2002**, *2*, 43.
(19) Elteto, K.; Lin, X. M.; Jaeger, H. M. *Phys. Rev. B* **2005**, *71*, 205412.
(20) Day, A. R.; Snyder, K. A.; Garboczi, E. J.; Thorpe, M. F. *J. Mech. Phys. Solids* **1992**, *40*, 1031.
(21) Wang, G.; Al-Ostaz, A.; Cheng, A. H. D.; Mantena, P. R. *Comput. Mater. Sci.* **2009**, *44*, 1126.
(22) Georgantzinos, S. K.; Giannopoulos, G. I.; Anifantis, N. K. *Mater Design* **2010**, *31*, 4646.
(23) Jiang, C. Y.; Tsukruk, V. V. *Adv. Mater.* **2006**, *18*, 829.